Engineering of three-dimensional pre-vascular networks within fibrin hydrogel constructs by microfluidic control over reciprocal cell signaling

Barbara Bachmann [⊥,1, 2, 3, 4], Sarah Spitz [⊥,1, 4, 5], Mario Rothbauer [⊥,1], Christian Jordan[1], Michaela Purtscher[6], Helene Zirath[1], Patrick Schuller[1], Christoph Eilenberger[1], Syed Faheem Ali[1,3,4], Severin Mühleder[2,3,4], Eleni Priglinger[2,4], Michael Harasek[1], Heinz Redl[2,3,4,5], Wolfgang Holnthoner[2,3,4] and Peter Ertl[*1,3,4]

[1] Faculty of Technical Chemistry, Institute of Applied Synthetic Chemistry, Institute of Chemical Technologies & Analytics, Vienna University of Technology, Austria

[2] AUVA Research Centre, Ludwig Boltzmann Institute for Experimental and Clinical Traumatology, Austria

[3] Kompetenzzentrum für MechanoBiologie (INTERREG V-A AT-CZ ATCZ133), Austria

[4] Austrian Cluster for Tissue Regeneration, Austria

[5] Trauma Care Consult GmbH, Vienna, Austria

[6] Department of Biochemical Engineering, University of Applied Sciences Technikum Wien, Vienna, Austria

[⊥]These authors contributed equally to the present work

[*]Correspondence: peter.ertl@tuwien.ac.at

ABSTRACT

Reengineering functional vascular networks *in vitro* remains an integral part in tissue engineering, since the incorporation of non-perfused tissues results in restricted nutrient supply and limited waste removal. Microfluidic devices are routinely used to mimic both physiologic and pathologic vascular microenvironments. Current procedures either involve the investigation of growth factor gradients and interstitial flow on endothelial cell sprouting alone or on the heterotypic cell-cell interactions between endothelial and mural cells. However, limited research has been conducted on the influence of flow on co-cultures of these cells. Here, we exploited the ability of microfluidics to create and monitor spatiotemporal gradients to investigate the influence of growth factor supply and elution on vascularization using static as well as indirect and direct flow setups. Co-cultures of human adipose-derived stem/stromal cells and human umbilical vein endothelial cells embedded in fibrin hydrogels were found to be severely affected by diffusion limited growth factor gradients as well as by elution of reciprocal signaling molecules during both static and flow conditions. Static cultures formed pre-vascular networks up to a depth of 4 millimeters into the construct with subsequent decline due to diffusion limitation. In contrast, indirect flow conditions enhanced endothelial cell sprouting but failed to form vascular networks. Additionally, complete inhibition of pre-vascular network formation was observable for direct application of flow through the hydrogel with decline of endothelial cell viability after seven days. Using finite volume CFD simulations of different sized molecules vital for pre-vascular network formation into and out of the hydrogel constructs, we found that interstitial flow enhances growth factor supply to the cells in the bulk of the chamber but elutes cellular secretome, resulting in truncated, premature vascularization.

INTRODUCTION

A major issue in tissue engineering is the formation of necrotic cores inside biological structures due to limited diffusion of oxygen and nutrients to tissue regions beyond 200-400 µm. One promising strategy to overcome apparent oxygen and nutrient deficiencies is based on the integration of lumenized and perfused vessels to promote long-term viability of tissue-engineered constructs.[1] Over the last decade, generation of vascularized tissues has steadily improved enabling controlled nutrient supply and waste removal to and from the engineered construct through blood vessel-like networks.[2, 3] From a physiological point of view, blood vessels are generally formed by two distinct mechanisms being vasculo- and angiogenesis.[4] While vasculogenesis refers to the *de novo* formation of blood vessels during embryonic development, angiogenesis requires a pre-existing vasculature, which can be extend by sprouting endothelial cells.[5] Additionally, mural cells such as vascular smooth muscle cells and pericytes actively take part in vessel maturation and stabilization.[6] While smooth muscle cells form concentric layers around arteries and veins, pericytes partially envelope smaller sized structures including arterioles, capillaries and venules.[7] Coordination of endothelial cell sprouting is therefore guided by both reciprocal cell signaling events and heterotypic cell-to-cell contact. Similar sprouting behavior has also been observed in the presence of adipose and bone-marrow derived mesenchymal stem cells, which are known to mimic mural cells through heterotypic cell-cell interactions with endothelial cells.[6, 8, 9] Mesenchymal stem cells secrete numerous factors including vascular-endothelial growth factor (VEGF) and hepatocyte growth factor (HGF) that not only contribute to endothelial cell survival and proliferation, but also promote the formation of pre-vascular structures *in vitro*.[8, 10, 11] Although the importance of reciprocal cell signaling on endothelial cell sprouting has been extensively studied over the years[6], little is still known on the influence of growth factor gradients, which are inherently present in any natural and engineered tissue construct.

To gain a deeper understanding of the modulating effect of spatio-temporal gradients on the formation of pre-vascular networks, we have developed three different microfluidic devices that allow precise control over nutrient supply from predefined entry points to a 3D-hydrogel based co-culture system. Microfluidic cell culture systems are ideally suited to study vascular biology due to the inherent ability to control the respective microenvironment.[12-17] For instance, 2D microfluidic endothelial cell cultures systems have been used to elucidate the

impact of growth factor gradients in intra- and extravasation of cancer cells[18-20] as well as VEGF[21, 22] and angiopoietin-1 (ANG-1) gradients in endothelial cell sprouting.[21] In addition to demonstrating the importance of VEGF gradients for the formation of blood vessels,[23, 24] microfluidic devices are routinely employed to provide physiologically relevant shear and interstitial flow regimes.[25] As an example, changes in endothelial cell morphology, phenotype and proliferative capacity have been reported for increasing shear conditions ranging up to 130 dyn cm^{-2}.[26] While under physiological shear stress of 0.1 dyn cm^{-2} to 3 dyn cm^{-2} a decrease in endothelial sprouting has been reported,[23] shear restriction and the presence of interstitial flow velocities between 1 µm/s and 35 µm s^{-1}, in turn, have shown to positively affect vasculo- and angiogenesis.[23, 27, 28] Although, in the absence of supporting cells these microfluidic endothelial cell culture systems failed to recapitulate the physiological architecture of microvessels in interstitial tissue, these studies still demonstrated that growth factor gradients may influence sprouting. Interestingly, all existing perfused microvascular networks based on co-culture of endothelial cells and mural cells did not consider apparent wash out effects and gradients of soluble growth factors during interstitial flow conditions.[20, 29, 30] Whereas current microfluidic strategies mainly focus on engineering perfusable vascular networks for establishing tumor models[20, 31] or on engineering bigger vessel structures for studying flow effects on endothelial barrier functions[32], we aimed to utilize microfluidics for fine tuning of vascularization by precisely controlling growth factor gradients and flow profiles. In contrast to most previously reported featuring cultivation chambers in the range of one to two millimeters with focus on establishing a perfusable network anastomosed to the microfluidic channel, the goal of this study was to establish bigger constructs for potential applications in tissue engineering. Hence, the microfluidic chambers greatly vary from previously published vasculature-on-chip in chamber size as well as hydrogel boundary surface.

To close this knowledge gap and to gain a deeper understanding of the relationship between heterotypic cell-to-cell interactions and reciprocal cell signaling during initial endothelial cell sprouting, a dual *in vitro* and *in silico* strategy is employed to describe the effects of spatial depletion of growth factors on the formation of a vascular network. In our experimental approach three microfluidic 3D co-culture systems, which contain adipose-derived stem cells as supporting cells and human umbilical vein endothelial cells embedded in a fibrin matrix, are used to evaluate vascular network area coverage and average microvessel length over a seven

day cultivation period Similar to recent publications in the field[25, 31], an initial vascular network formed after five days of culture with a mature vascular network after seven days. The microfluidic biochips are designed either for indirect and lateral perfusion or direct flow conditions to establish various gradients in 1 mm, 3 mm and 8 mm thick 3D vascular co-culture systems. Additional finite volume CFD simulations are performed to characterize transport phenomena and distance-relationships of signaling molecules and growth factors of increasing sizes ranging from 10 kDa, 20 kDa, 40 kDa to 500 kDa in the absence and presence of varying interstitial flow conditions. Since the individual and combinatorial biophysical constraints such as interstitial flow, size-dependent gradients and tissue dimension are key in vascular network formation, a better understanding of their modulating effects may provide new insight into angiogenesis, tissue regeneration and cancer biology.

MATERIALS & METHODS

Device Fabrication

Three microfluidic devices were used for characterization of tube formation under static or fluid flow conditions. Two of the devices had a circular chamber adjacent to a medium channel (see Figure 1). Microstructures were fabricated using polydimethylsiloxane (PDMS, Sylgard® 184 Silicone Elastomer Kit, Down Corning) by soft lithography from 3D-printed molds (imaterialise). After polymerization, the PDMS was bonded to glass slides using air plasma (Harrick Plasma, High Power, 2 min) and sterilized with 70% ethanol before use. In turn, the microfluidic biochip designed for direct perfusion through hydrogel (see Figure 4a) was manufactured using a PDMS-sheet cutter (CAMM-1 GS-24, Roland DGA). After cutting the microchannel network into PDMS membranes, the fluidic layer was sandwiched between two glass slides, sealed via air plasma activation and treated with 3% (3-Aminopropyl) triethoxysilane (APTES; Sigma Aldrich) solution for one hour. The assembled microfluidic biochips were sterilized (70% ethanol), rinsed with DI for a period of 30 min and coated with 10 mg/mL fibrinogen solution overnight.

Cell Culture and Device Seeding

Isolation of human adipose-derived stem cells (ASC) as well as human umbilical vein endothelial cells (HUVEC) was carried out as previously described[33, 34] following the approval of the ethics committees (state of Upper Austria and the AUVA) and written donor consent. Harvested cells were maintained in fully supplemented endothelial cell growth medium 2 (EGM-2, PromoCell)

with 5% fetal calf serum until passage 5 to 9. Retroviral transfection of GFP-HUVECs was carried out as previously published.[35, 36] Prior cell seeding into microfluidic devices, fibrin hydrogel (TISSEEL®, Baxter) with a final concentrations of 2,5 mg/mL fibrinogen, 1 U/mL thrombin, and $5*10^5$ cells/mL per cell type was loaded into the hydrogel chambers and polymerized for 45 minutes. Cell cultivation was carried out in the presence of fully supplemented EGM-2 medium under static conditions (exchange of medium every other day) and constant perfusion over a period of 7 days with four replicas per condition. Adipose-derived stem cell conditioned medium was generated by seeding 3500 cells/cm^2 and collecting secretome after three days of incubation. Non-treated controls were similarly incubated in culture flasks without cells. For stop-flow experiments, co-cultures were statically cultivated for three days before initiation of flow.

*Finite volume CFD simulation*A multipurpose finite volume CFD code was used for solving the flow problems. The geometries were split in hexahedral control volumes, an example grid is presented in Supplementary Figure 1A. Second or higher order discretization was selected for all flow variables as well as for the species equations. To ensure physically correct transient solutions, the time step size was selected to guarantee a maximum Courant number Co < 1 within the flow domain over the whole run time of up to 18 h. Wall boundaries were treated as ideally smooth, no slip boundary conditions were selected for all surfaces. The inlet of the flow geometry was set to mass flow inlet with a plug flow velocity profile, the outlet was set to pressure outlet at a standard pressure of 1 atm (101325 Pa) with the flow considered to be isothermal. For simplicity, Newtonian fluid behavior was assumed with a constant dynamic viscosity and constant density. As the concentrations of the dissolved species in the fluid are low, the properties of the solvent, water, have been used for the simulation (ρ = 998 kg/m^3, η = 0.001003 Pa*s). The diffusion coefficients for the tracer components have been set according to measurements or literature values, assuming a dilute solution. Tracers at the flow inlet were added as step functions at the initial time T = 0 s, at the same time a constant tracer saturation of the hydrogel zones were set as starting values for the simulation runs. In addition to the tracer species, a non-diffusing scalar was tracked for calculation of the residence time distributions, an example can be found in S1B. The maximum Reynolds number Re within the geometry was << 1, therefore laminar flow was assumed with no boundary layer grid. The

hydrogel regions were approximated as porous zones with constant porosities of ε = 0.99 and isotropic viscous resistances of $R = 6.67.10^{-12}$ 1/m².

Data Analysis

All microfluidic devices were analyzed on day 7 based on green fluorescence intensities obtained from transfected HUVECs using AngioTool64 software (Version 0.6a (02.18.14)) to determine network parameters as described elsewhere.[37]

RESULTS AND DISCUSSION

Impact of hydrogel volume and diffusion distances on reciprocal signaling during pre-vascular network formation

Microfluidic devices similar in design but consisting of differently sized hydrogel chambers ($Ø_1$= 3 mm, $Ø_2$ = 8 mm) are used to investigate tube formation, vessel length and area covered throughout the hydrogel in the presence of growth factor gradients. Figure 2 shows the impact of growth factor depletion on vascular network formation caused by diffusion-distance limitation and the elution of molecules produced by stem cells as well as endothelial cells during medium replacement. Results shown in Figure 2A and SI Figure xx revealed that vascular network formation occurred homogeneously throughout the smaller cultivation chamber ($Ø_1$= 3 mm, V = 7.5µL), covering approx. 9% of the entire growth volume with 15 to 20 junctions per mm^2. Since the average vessel length increased from 297 ± 26 µm within the first 1 mm to 439 ± 60 over a 3 mm distance into the cultivation chambers, sufficient supply of nutrients is provided throughout the whole cultivation chamber. In turn, results shown in Figure 2B point at the presence of a biochemical gradient, since vascular network parameters varied greatly throughout the 8 mm long (V = 100 µL) fibrin hydrogel construct. Within the first three millimeters distance from the medium supply channel, peak values for vessel area coverage of 40.4 ± 5.9 %, an average vessel length of 2.05 ± 0.94 mm and 22 ± 2 junctions per mm^2 are found. Between 3 mm and 8 mm distance, however, the quality of pre-vascular network formation declined gradually resulting in an average reduction of vessel area to 2.5 ± 2,2%, a vessel length of 0.18 ± 0.25 mm and 2.19 ± 0.1 junctions mm^{-2}.

To gain a better understanding of the underlying mechanisms responsible for the distance-dependent decline in the quality of pre-vascular network, fluorescently labelled dextran similar

in size as proangiogenic molecules including a 10 kDa dextran (e.g. EGF and IGF), a 20 kDa dextran (e.g. ß-FGF and PDGF) and a 40 kDa dextran (e.g. VEGF and Ang-1/-2) as well as FITC-dextran with 500 kDa in size was chosen as a reference molecule to visualize gradient formation inside the fibrin hydrogel constructs under static conditions. Based on these initial fluorescence imaging results (Supplementary Figure xx and yy), finite volume CFD simulations were performed to determine the distribution of differently-sized biomolecules inside the hydrogel volume. Figure 3A shows that approx. 30% of proangiogenic biomolecules with 40 kDa in size and 50% of smaller molecules are readily delivered within 12 hours to cells residing up to three millimeters inside the hydrogel construct. This is followed by the formation of a steep gradient starting around 3 mm hydrogel distance where only 10% of 20 kDa biomolecules but hardly any 40 kDa sized proangiogenic factors can reach deeper regions of the fibrin hydrogel. Any larger biomolecules only diffuse up to a distance of 2 mm reaching approx. of 5% mass after a 12 h period. Additionally, the removal of secreted biomolecules and elution into the medium supply channel was simulated to estimate the distribution of cell signaling molecules within the fibrin hydrogel construct. Results shown in Figure 3B indicate that over 80% of secreted biomolecules are eluted from the first millimeter and 50 % are still eluted from up to three millimeters inside the fibrin construct. In other words, microfluidic hydrogel volumes below 5 µL are prone to elution of proangiogenic factors, thus severely impeding reciprocal cell-cell signaling events.

Overall, our simulation results correlate well with experimental differences observed invascular network formation using microfluidic co-cultures of adipose-derived stem cells with endothelial cells, indicating that distance between 2 to 3 mm inside a hydrogel reaches optimum equilibrium between nutrient supply and elution of metabolites for pre-vascular network formation in static culture conditions. Since the 8 mm diameter hydrogel chamber design displayed gradient-dependent network formation, it was selected for subsequent flow experiments.

Impact of direct and indirect interstitial fluid flow on pre-vascular network formation

In addition to diffusion-limited supply of nutrients, interstitial flow conditions can also influence vascular network formation due to the increased elution of secreted biomolecules. To study the effects of direct and indirect fluid flow on pre-vascular network formation, two different microfluidic geometries shown in Figure 4 are employed in subsequent experiments. In the first

microfluidic configuration (right panel of Fig. 4) indirect interstitial flow conditions are established by directing the medium flow alongside the hydrogel interface at a velocity of 3 µm/s, whereas the second microchip design (left panel of Fig. 4) was adjusted to reduce hydrogel resistance and increase hydrogel anchorage to enable direct flow through the hydrogel. Results of our lateral flow direction study revealed that microfluidic ASCs/HUVEC co-cultures embedded in 8 mm fibrin hydrogel constructs started to form vascular connections already at day 3. Since apparent vascular network morphologies improved over the following 4 days in culture, sufficient supply of reciprocal signaling of proangiogenic growth factors is provided during indirect medium perfusion. In contrast, fluid flow forced through the fibrin hydrogel construct using our second microfluidic configuration (left panel of Fig.4) resulted in endothelial cell alignment in direction of the fluid flow with no evidence of pre-vascular network formation at day 3. Even more striking, complete loss of endothelial cell viability occurred by day 7 under direct interstitial fluid flow conditions. Additionally, finite volume CFD simulations (see Supplementary Video 1) revealed that direct fluid flow through a hydrogel results in complete elution of pro-angiogenic growth factors from the perfused region already after 120 s, thus eliminating reciprocal cell signaling and the formation of vascular structures. In other words, secretion of proangiogenic growth factors from the adipose-derived stem cells plays a key role in the initial phase of vascular network formation, while forced fluid flow through a hydrogel construct may be beneficial in maturation of preformed lumenized vessels.

Interstitial flow enhances sprouting but lessens network maturation

Since reciprocal cell-cell signaling is an important part during the onset and formation of pre-vascular networks, additional finite volume CFD simulations were performed to assess the distribution of proangiogenic growth factors in fibrin hydrogel constructs. *In silico* results shown in Figure 5 indicate that during indirect lateral flow conditions sufficient growth factors are present over the complete hydrogel distance, where 50% of 20 kDa sized molecules reach 4 mm and 40% diffuse up to 6 mm into the hydrogel within a period of 12 hours. Additionally, Figure 5A shows that approx. 50% of biomolecules ranging from 10 – 20 kDa in size are delivered in a similarly fashion to static cultures. It is important to note, however, that slightly higher biomolecule concentrations in the deeper regions of the hydrogel construct could be achieved in the presence of lateral fluid flow. Interestingly, lateral fluid flow did not increase the penetration depth of 40 kDa and 500 kDa biomolecules after 12 hours of perfusion.

Furthermore, elution of proangiogenic growth factors from the fibrin hydrogel construct is significantly enhanced for smaller biomolecules sizes with complete removal from the first millimeter distance (see Figure 5B), while bigger sized molecules displayed similar distributions as static cultivation.

In a next set of experiments, network area coverage, vessel length and number of junctions of microfluidic *in vitro* co-cultures of stem cells and endothelial cells were evaluated to assess the quality of vascular network formation in the presence of physiologically-relevant fluid flow rates that resemble interstitial flow regimes. Figure 6A shows a cross-section analysis of the 3D-cultivation chambers where images of endothelial tube formation are compared, revealing good agreement with above *in silico* results. While endothelial cell alignment along the flow direction is found within the first millimeter where highest flow rates are present, premature vascular connections started to form 2 mm inside the hydrogel exhibiting a vessel area coverage of 5.11 ± 1.42%, 51 ± 12 junctions mm^{-2} and an average vessel length of 0.066 ± 0.008 mm. In turn, within deeper regions around 4 mm inside of the hydrogel construct, vascular network formation improved markedly featuring a vessel area of 12.07 ± 1.21 %, 155 ± 16 junctions mm^{-2} and an average vessel length of 0.16 ± 0.02 mm. This improved vascular structure quality suggests efficient nutrient delivery to the entire hydrogel volume, while simultaneously retaining secreted cell signaling molecules, thus promoting homogenous vascular network formation.

In a final comparative analysis, vascular network formation in the presence of varying concentration gradients was investigated to assess the impact of size-depended growth factor distribution inside the hydrogel construct. Additionally, we investigated whether preconditioning of culture medium in stem cell secretome or application of a stop-flow regime alters vascular network formation. While gradients of small biomolecules (10 kDa and 20 kDa) are found using static conditions, concentration gradients of larger bioactive compounds (40kDa) are readily established using indirect perfusion set up. Results of our comparative study are summarized in Figure 7 where size-dependent biomolecule distribution and vascular network formation of ASC and HUVEC co-cultures embedded in fibrin hydrogels is analyzed. Results in Figure 7A illustrate that the distribution of biomolecules in the range of 10 kDa and 20 kDa differs between 20% to 40% over a distance of 1, 3 and 6 mm inside a hydrogel construct

in the presence of indirect perfusion. These phenomena can mainly be attributed to the elution and removal of smaller molecules from the hydrogel during lateral flow conditions. The evaluation of the quality of the vascular structures over the distance in the absence and presence of interstitial flow are shown in Figure 7B. While lateral perfusion of the fibrin-hydrogel construct led to improved endothelial sprouting events, reduced vessel length and network area coverage particular inside deeper regions (< 4 mm) are found compared to static conditions. Although dynamic culture conditions resulted in overall lower vascular network quality values, the obtained vascular morphology displayed a higher degree uniformity and regularity throughout the fibrin hydrogel construct. These results point at the mitigating effect of local concentration of proangiogenic biomolecules, which is governed by supply of nutrients, maintenance of secretome and elution of metabolic waste products. Further experiments using ASC conditioned medium to elucidate the effect of growth factor elution showed an improvement in network characteristics, visible in Figure 7D. Preconditioning of culture medium for three days resulted in higher network area coverage, increased number of junctions and longer overall vessel length. Finally, we hypnotized that application of flow after an initial static cultivation period of three days, allowing the formation of premature vascular connections before addition of flow, would enhance network characteristics. Indeed, we found that this stop-flow regime results in a denser network, an increased number of junctions and formation of longer vessels compared to a regular flow-only regime.

CONCLUSION

In the present work, we have investigated the influence of concentration gradients on the formation of vascular networks inside fibrin-hydrogel constructs containing human umbilical vein endothelial cells and adipose-derived stem cells. Using three different microfluidic 3D vascular co-culture models, the importance of biochemical gradients and reciprocal cell signaling events on endothelial sprouting was demonstrated in the absence and presence of indirect as well as direct flow conditions. Starting with single elongated cells at the edges of the hydrogel construct pre-vascular network formation started within 0.5 – 1 mm distance inside the fibrin hydrogel for all devices. In the absence of fluid flow, pre-vascular microvessels formation occurred predominantly inside 2 to 3 mm inside the fibrin construct followed by subsequent decline of vascular network quality. The observed asymmetry in endothelial sprouting events can be attributed to diffusional transport limitations of nutrients into deeper

zones of the vascular co-culture model. In turn, direct perfusion through fibrin construct resulted in endothelial cell alignment in flow direction during the first three days of culture, however no tube formation was obtained after 7 days. Indirect perfusion based on lateral flow direction showed significantly higher sprouting activity and uniformity throughout hydrogel construct, but also exhibited a reduced vascular network area coverage and decreased average microvessel length. To gain a deeper insight into gradient-mediated endothelial sprouting within a 3D matrix, an *in silico* assessment of size-dependent biomolecule distribution was performed. Our finite volume CFD simulations are based on experimental data derived from differently-sized and fluorescently-labeled dextrans. The selected size range of 10 kDa, 20 kDa, 40 kDa and 500 kDa soluble molecules correspond to the size of major signaling molecules and growth factors present during vascular network formation. Results from the finite volume CFD simulations on the distribution profiles of differently-sized proangiogenic molecules suggest that at least a 1:1 ratio between fresh nutrient supply and elution of reciprocal signaling molecules, produced locally within the hydrogel construct by the co-culture, is best suited to ensure efficient vascular network formation. This ratio corresponds to a balance of delivery of 50% fresh medium supplements and retention of 50% of reciprocal signaling molecules inside the fibrin hydrogel, a comparative graph of supply and elution in both static and dynamic conditions can be found in Figure 7A. In summary we found that establishment of growth factor gradients in the form of lateral fluid flow in the order of micrometers per second enhances endothelial cell sprouting and heterotypic cell-cell interactions facilitate initial network formationHowever, after vessel maturation spatio-temporally controlled direct perfusion of microvascular systems is of utmost importance to ensure proper endothelial phenotype. In other words, directed flows through a hydrogel construct are only beneficial in the presence of lumenized vessels, since adipose-derived stem cell secretome plays a key role in the initial phase of vascular network formation.

Acknowledgements:

This work was funded by the European Union's INTERREG V-A AT-CZ programme (ATCZ133), the European Union's Horizon 2020 research and innovation programme (685817), the City of Vienna Tissue Engineering International Project (MA 23, #14-06), and the Austrian Research Promotion Agency (FFG; 849791). Further, the authors thank Carina Huber-Gries for fruitful discussions.

REFERENCES

1. R. Costa-Almeida, P. L. Granja, R. Soares and S. G. Guerreiro, Eur Cell Mater **28**, 51-66; discussion 66-57 (2014).
2. M. Lovett, K. Lee, A. Edwards and D. L. Kaplan, Tissue Eng Part B Rev **15** (3), 353-370 (2009).
3. E. A. Phelps and A. J. Garcia, Curr Opin Biotechnol **21** (5), 704-709 (2010).
4. G. D. Yancopoulos, S. Davis, N. W. Gale, J. S. Rudge, S. J. Wiegand and J. Holash, Nature **407** (6801), 242-248 (2000).
5. W. Risau, Nature **386** (6626), 671-674 (1997).
6. K. Pill, S. Hofmann, H. Redl and W. Holnthoner, Cell Regen (Lond) **4**, 8 (2015).
7. K. Gaengel, G. Genove, A. Armulik and C. Betsholtz, Arterioscler Thromb Vasc Biol **29** (5), 630-638 (2009).
8. F. Verseijden, S. J. Posthumus-van Sluijs, P. Pavljasevic, S. O. Hofer, G. J. van Osch and E. Farrell, Tissue Eng Part A **16** (1), 101-114 (2010).
9. S. Merfeld-Clauss, N. Gollahalli, K. L. March and D. O. Traktuev, Tissue Eng Part A **16** (9), 2953-2966 (2010).
10. J. Rehman, D. Traktuev, J. Li, S. Merfeld-Clauss, C. J. Temm-Grove, J. E. Bovenkerk, C. L. Pell, B. H. Johnstone, R. V. Considine and K. L. March, Circulation **109** (10), 1292-1298 (2004).
11. S. Rohringer, P. Hofbauer, K. H. Schneider, A. M. Husa, G. Feichtinger, A. Peterbauer-Scherb, H. Redl and W. Holnthoner, Angiogenesis **17** (4), 921-933 (2014).
12. D. Wartmann, M. Rothbauer, O. Kuten, C. Barresi, C. Visus, T. Felzmann and P. Ertl, Frontiers in Materials **2** (60) (2015).
13. D. Sticker, S. Lechner, C. Jungreuthmayer, J. Zanghellini and P. Ertl, Anal Chem **89** (4), 2326-2333 (2017).
14. M. Rothbauer, H. Zirath and P. Ertl, Lab Chip **18** (2), 249-270 (2018).
15. M. Rothbauer, D. Wartmann, V. Charwat and P. Ertl, Biotechnol Adv **33** (6 Pt 1), 948-961 (2015).
16. M. Rothbauer, I. Praisler, D. Docter, R. H. Stauber and P. Ertl, Biosensors (Basel) **5** (4), 736-749 (2015).
17. Rosser JM., Olmos-Calvo I., Schlager M., Purtscher M., Jenner F. and E. P., J Cell Biol Cell Metab **2** (005) (2015).
18. K. Aizel, A. G. Clark, A. Simon, S. Geraldo, A. Funfak, P. Vargas, J. Bibette, D. M. Vignjevic and N. Bremond, Lab Chip **17** (22), 3851-3861 (2017).
19. I. K. Zervantonakis, S. K. Hughes-Alford, J. L. Charest, J. S. Condeelis, F. B. Gertler and R. D. Kamm, Proc Natl Acad Sci U S A **109** (34), 13515-13520 (2012).
20. J. S. Jeon, S. Bersini, M. Gilardi, G. Dubini, J. L. Charest, M. Moretti and R. D. Kamm, Proc Natl Acad Sci U S A **112** (1), 214-219 (2015).
21. Y. Shin, J. S. Jeon, S. Han, G. S. Jung, S. Shin, S. H. Lee, R. Sudo, R. D. Kamm and S. Chung, Lab Chip **11** (13), 2175-2181 (2011).
22. W. A. Farahat, L. B. Wood, I. K. Zervantonakis, A. Schor, S. Ong, D. Neal, R. D. Kamm and H. H. Asada, PLoS One **7** (5), e37333 (2012).
23. J. W. Song and L. L. Munn, Proc Natl Acad Sci U S A **108** (37), 15342-15347 (2011).
24. C. L. Helm, M. E. Fleury, A. H. Zisch, F. Boschetti and M. A. Swartz, Proc Natl Acad Sci U S A **102** (44), 15779-15784 (2005).
25. K. Haase and R. D. Kamm, Regen Med **12** (3), 285-302 (2017).
26. Q. Smith and S. Gerecht, Curr Opin Chem Eng **3**, 42-50 (2014).
27. Y. H. Hsu, M. L. Moya, C. C. Hughes, S. C. George and A. P. Lee, Lab Chip **13** (15), 2990-2998 (2013).
28. C. Bonvin, J. Overney, A. C. Shieh, J. B. Dixon and M. A. Swartz, Biotechnol Bioeng **105** (5), 982-991 (2010).
29. J. S. Jeon, S. Bersini, J. A. Whisler, M. B. Chen, G. Dubini, J. L. Charest, M. Moretti and R. D. Kamm, Integr Biol (Camb) **6** (5), 555-563 (2014).
30. S. Kim, H. Lee, M. Chung and N. L. Jeon, Lab Chip **13** (8), 1489-1500 (2013).

31. A. Sobrino, D. T. T. Phan, R. Datta, X. Wang, S. J. Hachey, M. Romero-López, E. Gratton, A. P. Lee, S. C. George and C. C. W. Hughes, Scientific Reports **6**, 31589 (2016).
32. W. J. Polacheck, M. L. Kutys, J. Yang, J. Eyckmans, Y. Wu, H. Vasavada, K. K. Hirschi and C. S. Chen, Nature **552**, 258 (2017).
33. S. Wolbank, A. Peterbauer, M. Fahrner, S. Hennerbichler, M. van Griensven, G. Stadler, H. Redl and C. Gabriel, Tissue Eng **13** (6), 1173-1183 (2007).
34. P. Petzelbauer, J. R. Bender, J. Wilson and J. S. Pober, J Immunol **151** (9), 5062-5072 (1993).
35. S. Muhleder, K. Pill, M. Schaupper, K. Labuda, E. Priglinger, P. Hofbauer, V. Charwat, U. Marx, H. Redl and W. Holnthoner, Stem Cell Res Ther **9** (1), 35 (2018).
36. L. Knezevic, M. Schaupper, S. Muhleder, K. Schimek, T. Hasenberg, U. Marx, E. Priglinger, H. Redl and W. Holnthoner, Front Bioeng Biotechnol **5**, 25 (2017).
37. E. Zudaire, L. Gambardella, C. Kurcz and S. Vermeren, PLoS One **6** (11), e27385 (2011).

Figure captions:

Figure 1 Schematic overview of the microfluidic device.

Figure 2 Fluorescence images of pre-vascular networks with quality parameters in fibrin-based hydrogel constructs seeded with adipose-derived stem cells and green-fluorescent endothelial cells for (A) 3 mm and (B) 8 mm hydrogel chamber diameter day 7 post seeding.

Figure 3 Finite element simulations of size-dependent molecule diffusion (A) and elution (B) for static cell culture conditions.

Figure 4 Influence of direct compared to orthogonal interstitial fluid flow on pre-vascular network formation.

Figure 5 Finite element simulations of size-dependent molecule diffusion (A) and elution (B) for indirect interstitial fluid flow.

Figure 6 (A) Fluorescence images pre-vascular networks and (B) quality parameters of adipose-derived stem cells (red) and umbilical vein endothelial cells (green) at interstitial fluid flow day 7 post seeding.

Figure 7 (A) Finite element simulations of biomolecule diffusion in static compared to dynamic cell culture conditions. (B) Comparison of pre-vascular network formation for static and dynamic culture conditions using microfluidic devices day 7 post seeding.

FIGURES

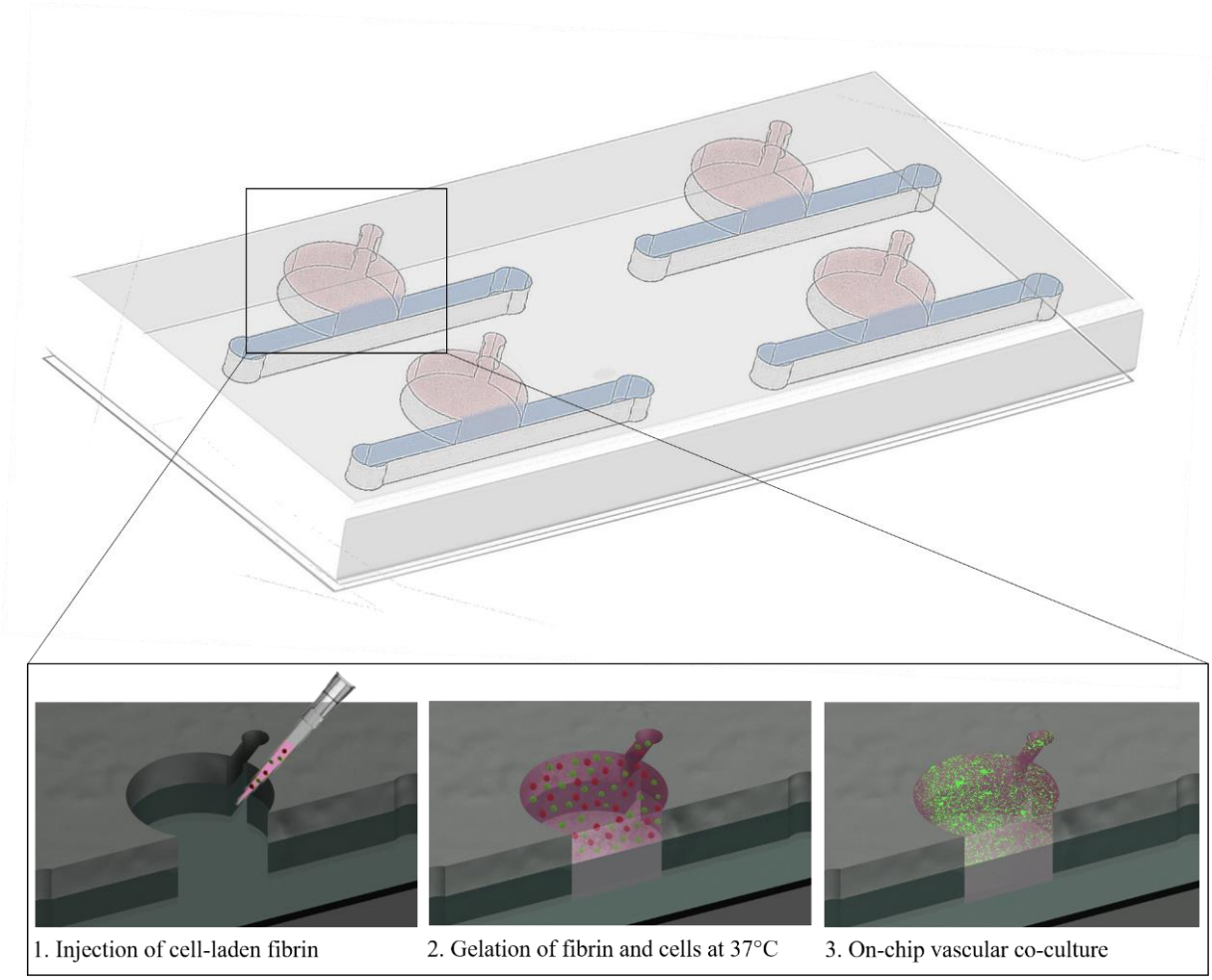

Figure 1

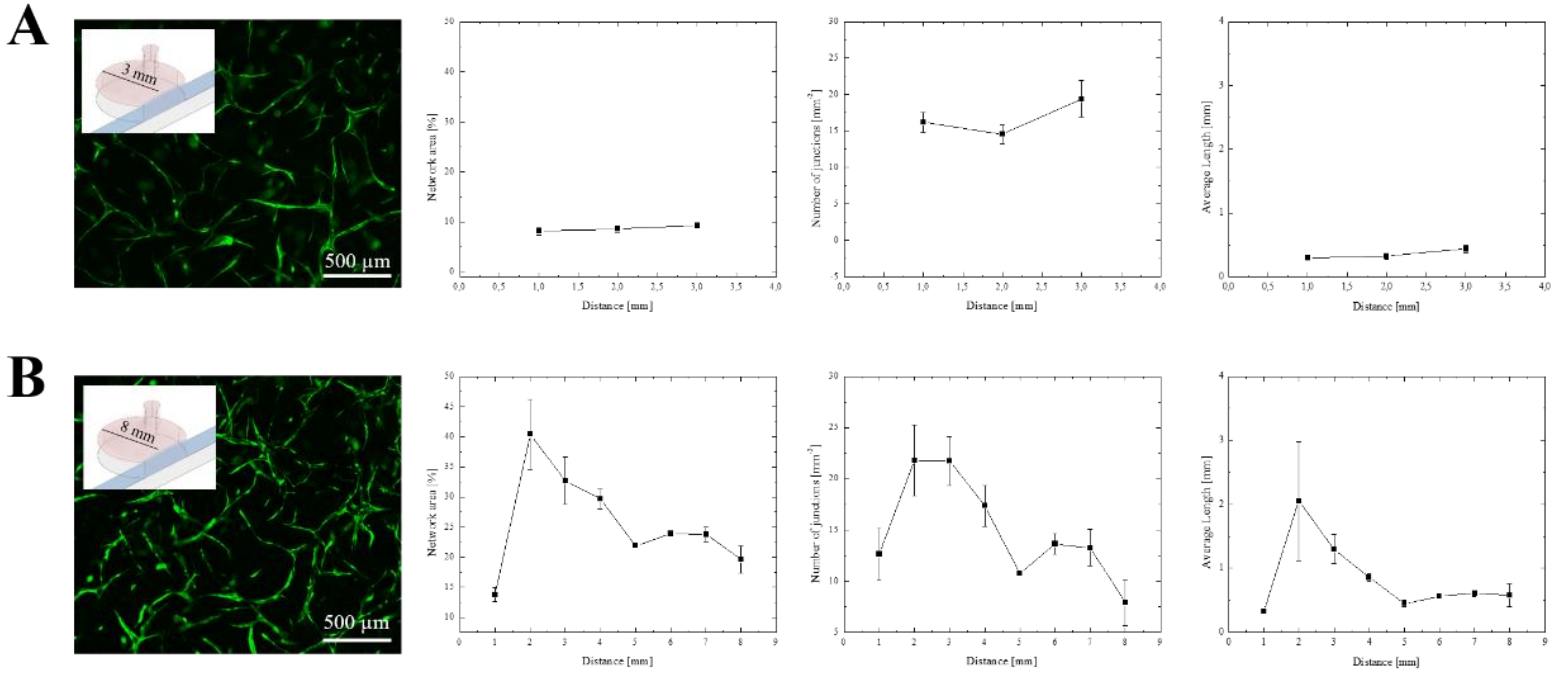
A
3 mm
500 µm
Network area [%]
Distance [mm]
Number of junctions [mm⁻²]
Distance [mm]
Average Length [mm]
Distance [mm]
B
8 mm
500 µm
Network area [%]
Distance [mm]
Number of junctions [mm⁻²]
Distance [mm]
Average Length [mm]
Distance [mm]

Figure 2

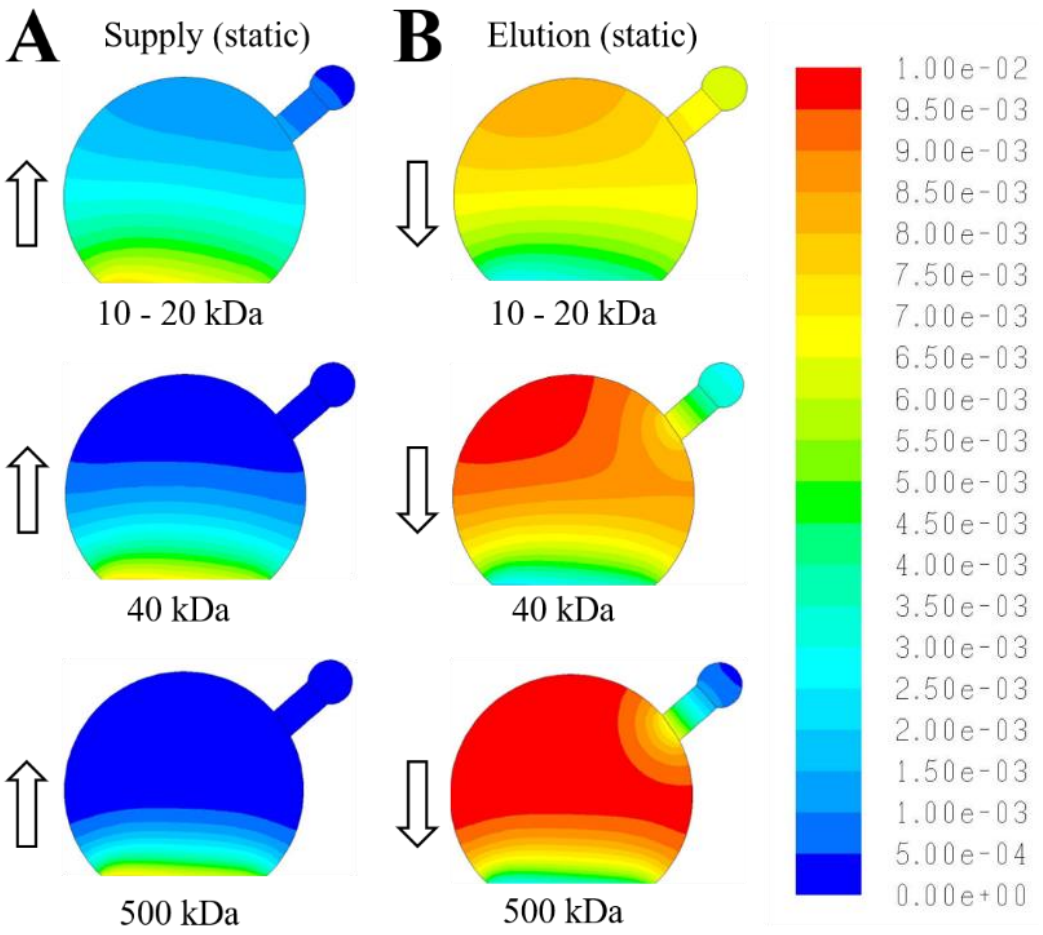
A
Supply (static)
B
Elution (static)
10 - 20 kDa
10 - 20 kDa
40 kDa
40 kDa
500 kDa
500 kDa
1.00e-02
9.50e-03
9.00e-03
8.50e-03
8.00e-03
7.50e-03
7.00e-03
6.50e-03
6.00e-03
5.50e-03
5.00e-03
4.50e-03
4.00e-03
3.50e-03
3.00e-03
2.50e-03
2.00e-03
1.50e-03
1.00e-03
5.00e-04
0.00e+00

Figure 3

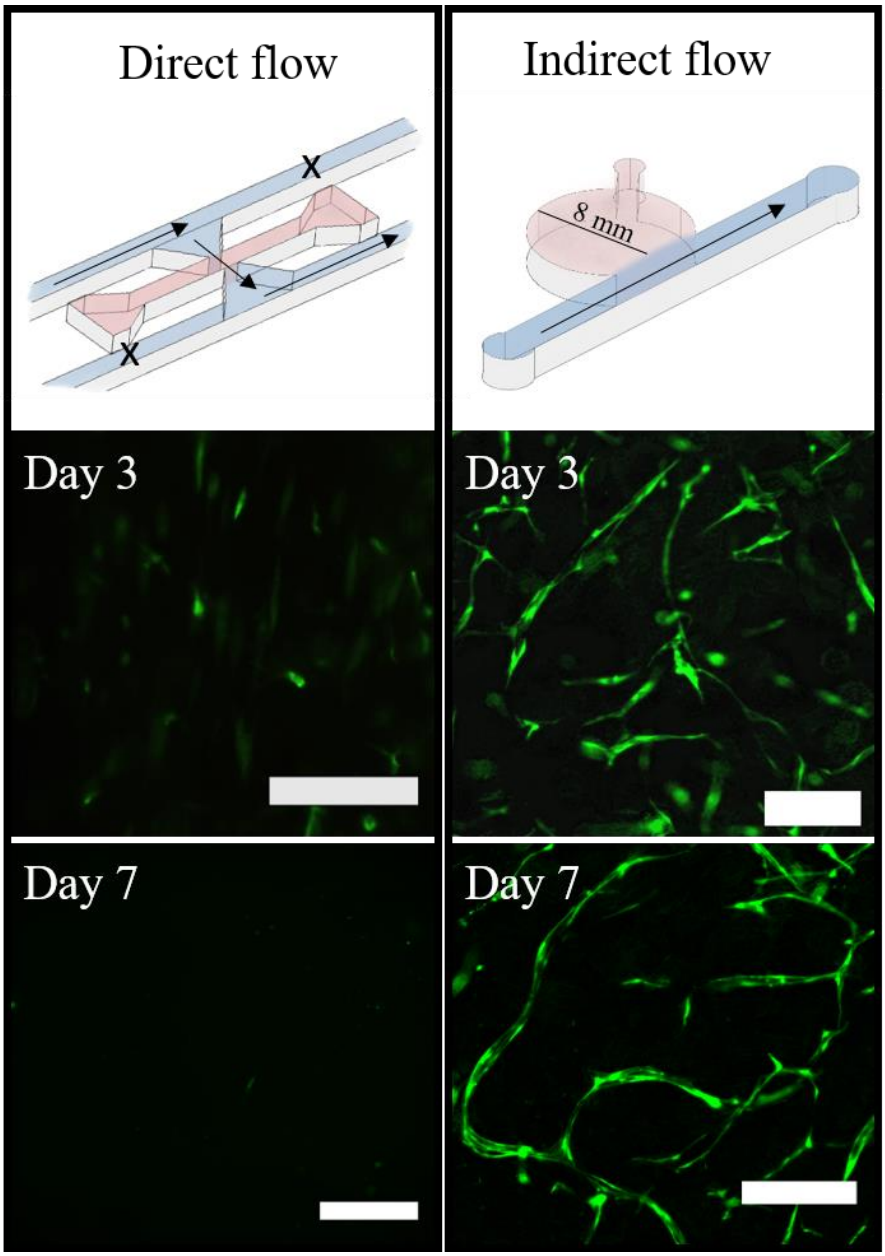

Figure 4

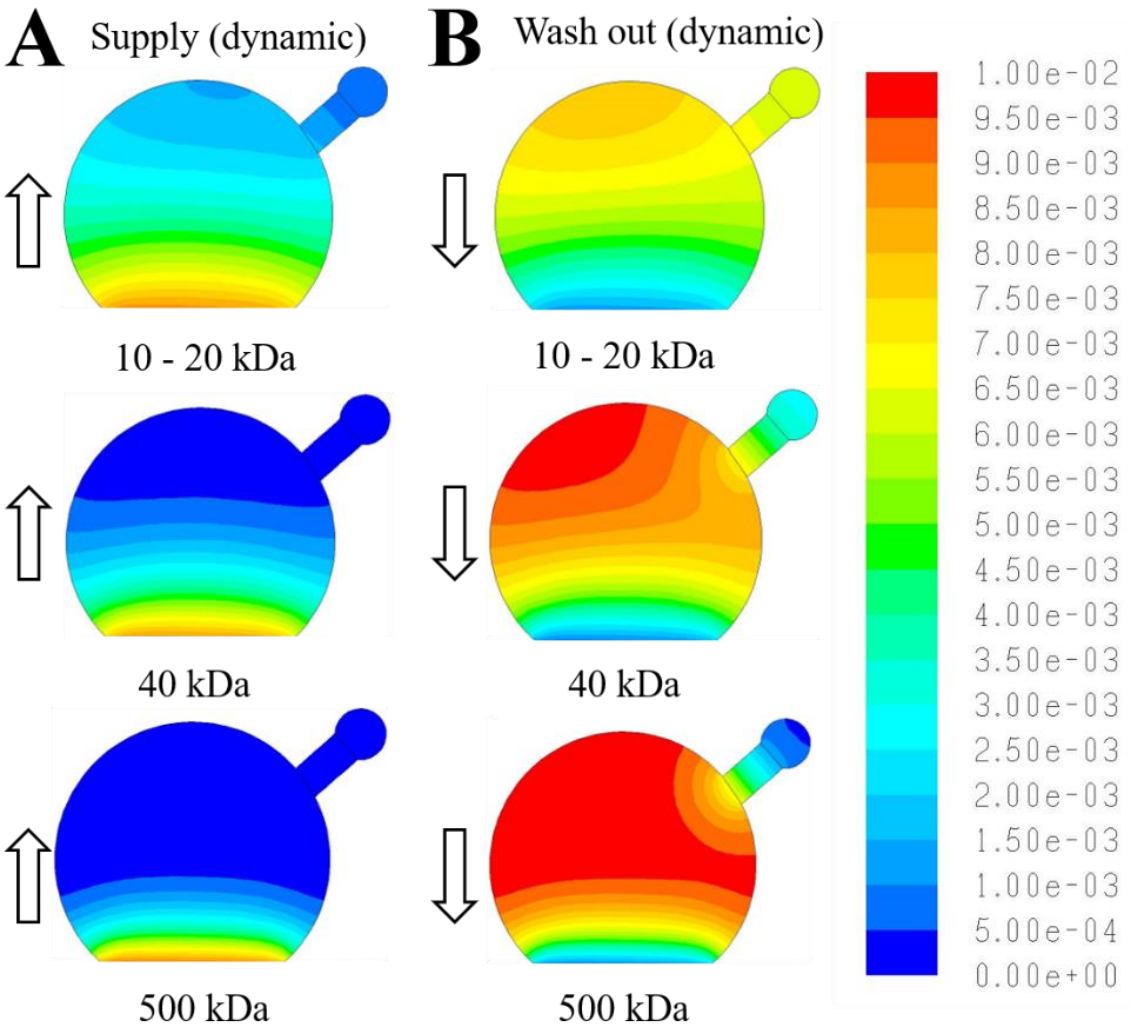
A
Supply (dynamic)
B
Wash out (dynamic)
10 - 20 kDa
10 - 20 kDa
40 kDa
40 kDa
500 kDa
500 kDa
1.00e-02
9.50e-03
9.00e-03
8.50e-03
8.00e-03
7.50e-03
7.00e-03
6.50e-03
6.00e-03
5.50e-03
5.00e-03
4.50e-03
4.00e-03
3.50e-03
3.00e-03
2.50e-03
2.00e-03
1.50e-03
1.00e-03
5.00e-04
0.00e+00

Figure 5

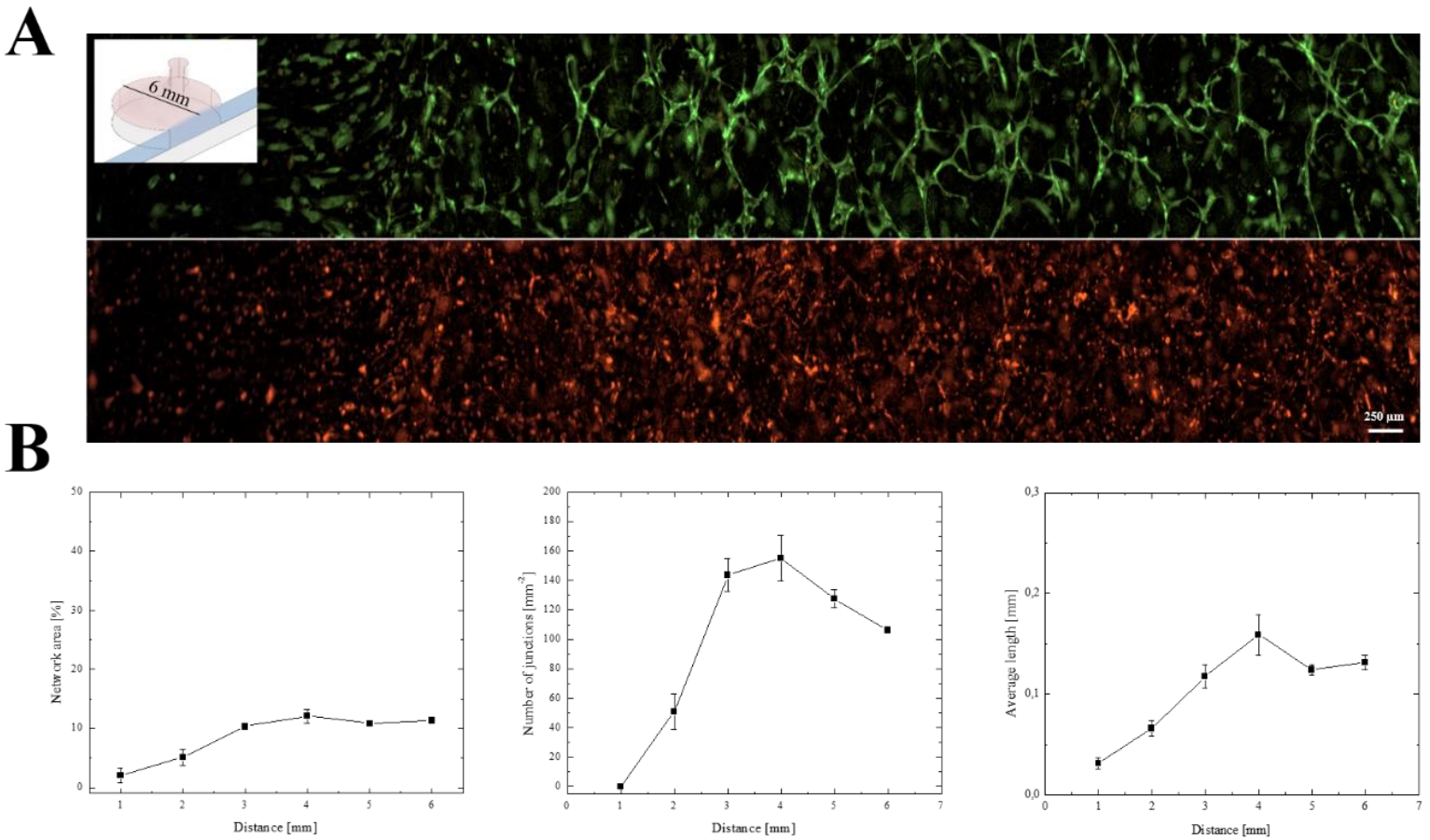
A
6 mm
250 µm
B
Network area [%]
Distance [mm]
Number of junctions [mm^{-2}]
Distance [mm]
Average length [mm]
Distance [mm]

Figure 6

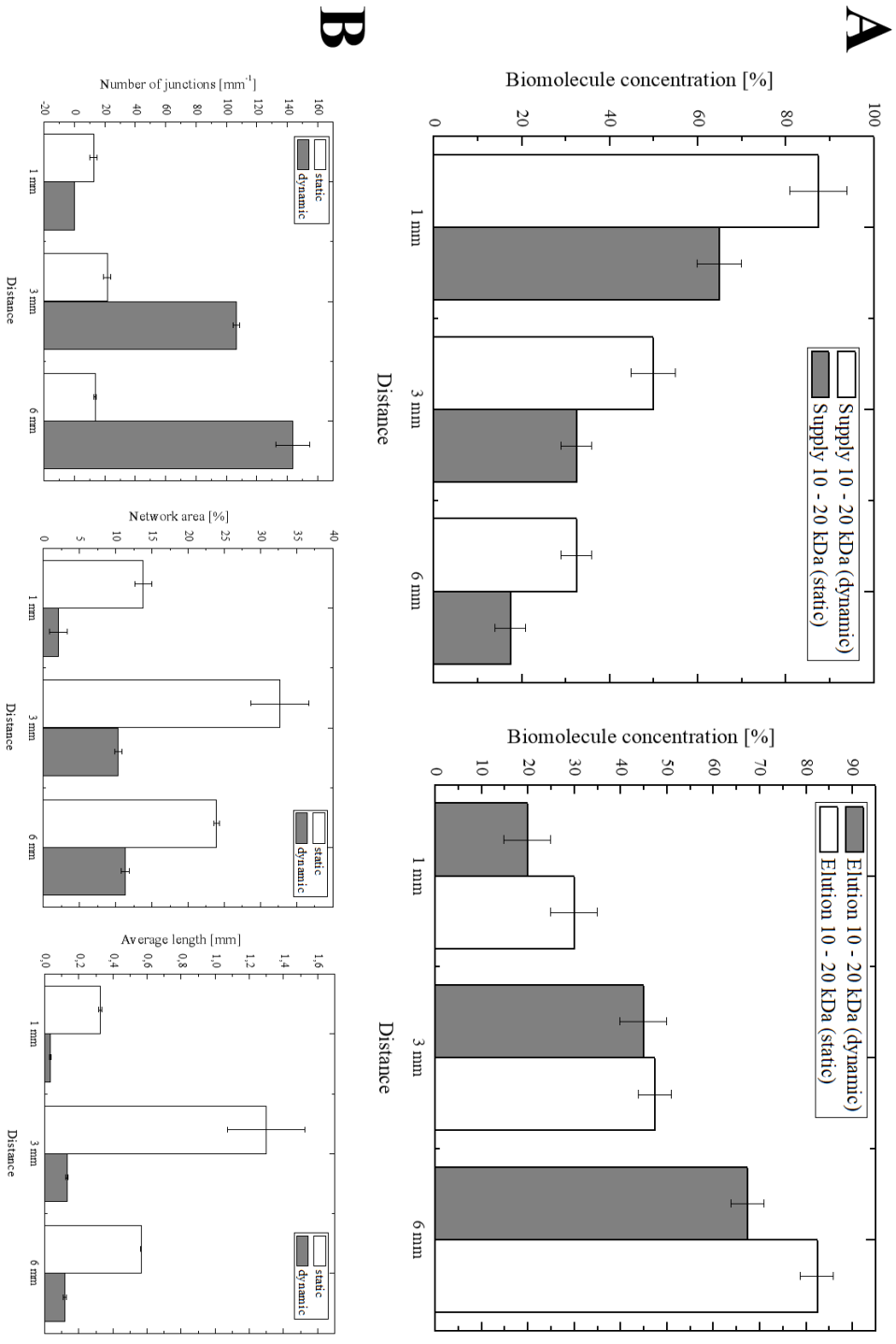
A
Biomolecule concentration [%]
Supply 10 - 20 kDa (dynamic)
Supply 10 - 20 kDa (static)
Distance
1 mm
3 mm
6 mm
Biomolecule concentration [%]
Elution 10 - 20 kDa (dynamic)
Elution 10 - 20 kDa (static)
Distance
B
Number of junctions [mm-1]
Network area [%]
Average length [mm]
static
dynamic

Figure 7

Supplementary Figure 1